

A central-moment multiple-relaxation-time collision model

Xiaowen Shan*

Department of Mechanics and Aerospace Engineering,

Southern University of Science and Technology,

Shenzhen, Guangdong 518055, China

Abstract

We propose a multiple relaxation time Boltzmann equation collision model by systematically assigning a separate relaxation time to each of the central moments of the distribution function. The Chapman-Enskog calculation leads to correct hydrodynamic equations. The thermal diffusion and viscous dissipation are mutually independent and Galilean invariant. By transforming the central moments into the absolute reference frame and evaluating using fixed discrete velocities, an efficient lattice Boltzmann (LB) model is obtained. The LB model is found to have excellent numerical stability in high-Reynolds numbers simulations.

* shanxw@sustc.edu.cn

I. INTRODUCTION

In the past three decades the lattice Boltzmann method (LBM) [1–3], particularly the lattice BGK (LBGK) single-relaxation-time (SRT) model [4–6], has gained a tremendous popularity in many areas of fluid mechanics. Despite the great success, a number of deficiencies have long plagued LBGK. The most noticeable ones are perhaps the fixed unity Prandtl number, the sometimes poor numerical stability, and the various forms of violations of the Galilean invariance. Aiming at eliminating, or at least alleviating, these deficiencies, a number of efforts have been made to improve the collision model, including the multiple-relaxation-time (MRT) model [7, 8] and its central-moment (CM) version [9], the “regularized” models [10–14], and the Hermite expansion based high-order MRT model [15, 16]. These models, suggested with their own purposes and assumptions, all enjoyed success of various degrees and shared the commonality that the moments of the distribution are individually manipulated. One of the aims of the present work is to offer a coherent view that can hopefully provide a theoretical framework within which the essence of the aforementioned models can be examined.

The unity Prandtl number is a well-known artifact of the BGK model which relaxes all moments at the same rate. A few remedies in continuum, *e.g.*, the ellipsoid-statistical BGK [17–19] and the Shakhov model [20] were suggested to introduce additional parameters in the target distribution so that the heat flux is decoupled from stress tensor. In the LB realm, McNamara *et al* [21] implemented a LB collision operator with a different eigenvalue for the third moments with respect to the *peculiar velocity* to adjust the thermal conductivity. In the MRT model of d’Humières *et al* [8, 22], the distribution function is decomposed into eigen-vectors corresponding to the lowest raw moments to each of which a separate relaxation time is assigned. Theoretically this should allow a variable Prandtl number. However, as the recovery of the heat equation requires accurate discrete representation of the third moments [23] which is not possible on the types of lattices that the MRT was developed with, the MRT was mostly advocated as a stability improvement. However, the idea of assigning a separate relaxation time to each of the moments was generalized to high-order LBM to allow a variable Prandtl number [15].

In practical simulations, the MRT model was observed to drastically improve the numerical stability at high Reynolds numbers [8, 24]. It is now generally agreed that this improvement is due to the filtering of the “ghost” modes that are not adequately represented by the discrete velocities [23]. Similar improvements was indeed achieved by the “regularized” models which

trim the under-resolved moments [10–12, 25]. More recently, the regularization approach was extended to high-order LB [13, 14, 26], leading to further enhanced numerical stabilities.

The problem of Galilean invariance has been known since the days of the lattice Gas Cellular Automaton (LGA) fluid models [1]. Due to discretization, the hydrodynamic equations differs from the Navier-Stokes-Fourier (NSF) equations by some velocity-dependent terms. Most of these problems have been fixed in the LBGK model [5, 6] except the so-called “cubic” error [27] which results in velocity-dependent viscosity and/or thermal diffusivity. This is now understood as being caused by not retaining sufficient moments when the BGK equation is discretized in velocity space and can be completely eliminated by using higher-order equilibrium distributions and lattices [23]. Partial removal of this error is also possible by explicitly correcting the incomplete third moments [28]. In the high-order MRT model, another violation of Galilean invariance emerged in the energy equation when the second and third moments are relaxed at different rates. More recently this error was removed by explicitly requiring the third moments to take a particular form that yields the NSF equations [16], in a similar fashion that the equilibrium distribution was modified for a similar purpose [5]. Nevertheless, it is not clear how this approach can be extended to the relaxation of higher-order moments.

The cascaded LB [9] (CLB) extends the MRT by performing moment relaxation in the reference frame moving with the fluid, leading to a cascade of equations where the relaxations of the higher moments involves those of the lower ones. Significant improvement of numerical stability has been observed in simulations [29] which is understandable as moment expansion in the relative frame, *i.e.*, *central moments* (CMs) expansion, intrinsically has a faster convergence and hence a better numerical performance. As the derivation of the CLB is rather involved, it is difficult to be extended beyond the second order to address the unity Prandtl number problem. Also, the complete restoration of Galilean invariance in the viscous term also requires correct handling of the third moments [23]. The viscosity observed in the simulation [9] does show a velocity-dependency despite its small achievable value. As far as this author is aware of, there hasn’t been any numerical evidence that CLB has corrected the cubic error.

Lastly, we note that in continuum kinetic theory, moment expansion is almost always in CMs [30]. However, to compute the CMs with discrete velocities *via* quadrature, the abscissas must be chosen in the moving frame and become variables themselves. Sun *et al* [31, 32] devised an *adaptive* LB in which the CMs are computed such way and fast convergence were indeed achieved. The downside is that a complicated particle streaming scheme involving inter-

polution has to be adopted. If the advantages of simple streaming-collision algorithm and linear advection are preferred, the discrete velocities must be fixed in the absolute frame.

Here, extending the ideas in Ref. [15], we derive a generic high-order MRT collision model by separate relaxation of the central moments. We first note that common to the MRT, regularizations, and cascaded collision models is the extraction of the moments from the discrete distribution function. Moments computed by discrete summation are not guaranteed to be the same as the corresponding velocity integrals in continuum. Namely, the equality:

$$\sum_{i=1}^d f(\xi_i) \xi_i \cdots \xi_i = \int f(\xi) \xi \cdots \xi d\xi, \quad (1)$$

may or may not hold depending on both the nature of f and the discrete velocities. In case it doesn't, the hydrodynamic equations of the discrete model must be re-derived, *e.g.*, by Chapman-Enskog (CE) calculation. Our formulation here is based on the previous works [33, 34] where the LB equation was formulated as a special velocity-space discretization of the continuous BGK equation. In the classic CE calculation of the BGK equation [35], the hydrodynamic equations depend only on the leading CM's of the distribution function instead of its entirety. Provided that the discrete velocities form a sufficiently accurate quadrature and the equilibrium distribution is a finite-order truncation of the Maxwellian, Eq. (1) is guaranteed up to certain order, and the hydrodynamic equations are guaranteed to be the same as those obtained from the continuous BGK equation. The derivation is simple, generic and lattice-independent. The obtained model has a tunable Prandtl number and Galilean invariant viscous and thermal dissipations. At the lowest order, the result of Ref. [16] is recovered. In addition, numerical stability similar to or better than those of the regularized models are achieved.

The work is organized as the following. Theoretical formulation is presented in Sec. II, where, after laying out necessary background, we first define a transform between the moments and the discrete distribution in Sec. II A. In Sec. II B Some previous LB collision models are examined within this framework. In Sec. II C the general conditions for the collision term to yield NSF equations are obtained by examining the CE procedure with BGK collision operator [35, 36]. Using these conditions, a generic high-order MRT collision model is then constructed in terms of its Hermite expansion. Numerical verifications are provided in Sec. III, and further discussions and conclusions are in Sec. IV. Some relations between the moments and Hermite coefficients in the absolute and relative frames are given in Appendix A.

II. THEORETICAL DERIVATION

The LB equation can be viewed as the projection of the following continuous Boltzmann-BGK equation into a low-dimensional Hilbert space spanned by the leading Hermite polynomials [33, 34]:

$$\frac{\partial f}{\partial t} + \boldsymbol{\xi} \cdot \nabla f + \mathbf{g} \cdot \nabla_{\boldsymbol{\xi}} f = \Omega(f). \quad (2)$$

Here, f , $\boldsymbol{\xi}$ and \mathbf{g} are the single-particle distribution, the peculiar velocity and the external body force respectively, $\nabla_{\boldsymbol{\xi}}$ the gradient operator in velocity space, and $\Omega(f)$ the BGK single-relaxation-time (SRT) collision model [4]:

$$\Omega = -\frac{1}{\tau} [f - f^{(0)}], \quad (3)$$

and $f^{(0)}$ the Maxwellian:

$$f^{(0)} = \frac{\rho}{(2\pi\theta)^{D/2}} \exp \left[-\frac{|\boldsymbol{\xi} - \mathbf{u}|^2}{2\theta} \right], \quad (4)$$

where ρ , \mathbf{u} and θ are respectively the dimensionless fluid density, velocity, and temperature [34].

Hermite polynomials in high dimensions were extensively treated by Grad [37]. Throughout the paper, we use a slightly different notation which is standard in Tensor Analysis. First define the *symmetrization* operator:

$$\text{Sym}(\mathbf{A}) \equiv \frac{1}{r!} \sum A_{i_1 \dots i_r}, \quad (5)$$

where, \mathbf{A} is a rank- r tensor and the summation is over the $r!$ permutations of the r indexes. The *symmetric product* of two tensors, \mathbf{A} and \mathbf{B} , is denoted by \mathbf{AB} and defined as:

$$\mathbf{AB} \equiv \text{Sym}(\mathbf{A} \otimes \mathbf{B}), \quad (6)$$

where \otimes stands for the normal tensor product. The symmetric product has the following properties:

1. commutativity: $\mathbf{AB} = \mathbf{BA}$;
2. associativity: $(\mathbf{AB})\mathbf{C} = \mathbf{A}(\mathbf{BC})$;
3. distributivity: $(\mathbf{A} + \mathbf{B})\mathbf{C} = \mathbf{AC} + \mathbf{BC}$.

Hereinafter all tensor products are symmetric unless otherwise noted.

A. The discrete Hermite transform

Critical to our formulation of the MRT collision operator is the extraction of the velocity moments from the *discrete* distributions. For the hydrodynamic equations to be the NSF equations, we must ensure that the moments so obtained are exactly the continuum hydrodynamic moments, *i.e.*, Eq. (1) must hold. Similar to the Discrete Fourier Transforms (DFT), for a function that is a finite Hermite series, a transform between its moments and discrete function values can be defined *via* Gauss quadrature [38, 39]. First, the Hermite polynomials form an ortho-normal basis of the D -dimensional function space w.r.t. the inner-product $\langle f, g \rangle \equiv \int \omega f g d\xi$, where $\omega(\xi)$ is the weight function:

$$\frac{1}{(2\pi)^{D/2}} \exp \left[-\frac{|\xi|^2}{2} \right]. \quad (7)$$

For any function f such that f/ω is square-integrable, the following general Fourier series exists:

$$f(\xi) = \omega(\xi) \sum_{n=0}^{\infty} \frac{1}{n!} \mathbf{a}^{(n)} : \mathcal{H}^{(n)}(\xi), \quad (8)$$

where,

$$\mathbf{a}^{(n)} = \int f(\xi) \mathcal{H}^{(n)}(\xi) d\xi, \quad n = 0, \dots, \infty, \quad (9)$$

is the n -th Hermite coefficients, and ‘:’ denotes full tensor contraction. Since $\mathcal{H}^{(n)}(\xi)$ is a polynomial in ξ , $\mathbf{a}^{(n)}$ is essentially a combination of the velocity moments. For an N -th degree polynomials, $p(\xi)$, there exists a set of abscissas and associated weights, $\{\xi_i, w_i : i = 1, \dots, d\}$, such that:

$$\int \omega(\xi) p(\xi) d\xi = \sum_{i=1}^d w_i p(\xi_i). \quad (10)$$

Particularly, quadrature rules with abscissas coincide with a Bravais lattice, *aka* “on-lattice” quadratures, can be obtained by solving a *linear programming* problem [34, 40–43]. Consider the N -th order truncation of Eq. (8):

$$f_N(\xi) \equiv \omega(\xi) \sum_{n=0}^N \frac{1}{n!} \mathbf{a}^{(n)} : \mathcal{H}^{(n)}(\xi). \quad (11)$$

Obviously f_N/ω is an N -th order polynomial. Eq. (9) can be written as:

$$\mathbf{a}^{(n)} = \int \omega(\xi) \left[\frac{f_N(\xi) \mathcal{H}^{(n)}(\xi)}{\omega(\xi)} \right] d\xi. \quad (12)$$

Noting that the term inside the brackets is an $(N+n)$ -th degree polynomial, by Eq. (10) we have:

$$\mathbf{a}^{(n)} = \sum_{i=1}^d f_i \mathcal{H}^{(n)}(\xi_i), \quad n = 0, \dots, Q - N, \quad (13)$$

where ξ_i and w_i are respectively the abscissas and weights of a degree- Q quadrature rule, and:

$$f_i \equiv \frac{w_i f_N(\xi_i)}{\omega(\xi_i)} = w_i \sum_{n=0}^N \frac{1}{n!} \mathbf{a}^{(n)} : \mathcal{H}^{(n)}(\xi_i). \quad (14)$$

Eqs. (13) and (14) define an isomorphic transform between $\mathbf{a}^{(n)}$ and f_i , allowing the hydrodynamic moments to be exactly computed from the discrete distribution and *vice versa*.

As shown previously [34], f_i are exactly the discrete distribution of LB. By Eq. (13), the leading moments are the familiar expressions defining density, ρ , velocity, \mathbf{u} , and kinetic energy density, ϵ :

$$\rho = \sum_{i=1}^d f_i, \quad \rho \mathbf{u} = \sum_{i=1}^d f_i \xi_i, \quad \rho(u^2 + 2\epsilon) = \sum_{i=1}^d f_i \xi_i^2. \quad (15)$$

The dynamic equations for f_i are obtained by directly evaluating Eq. (3) at ξ_i . After space and time discretization, we can write the LBGK equation in the following form:

$$f_i(\mathbf{x} + \xi_i, t + 1) = (1 - \omega) f_i + \omega f_i^{(0)}, \quad (16)$$

where $\omega \equiv 1/\tau$ is the collision frequency. Writing $f_i = f_i^{(0)} + f_i^{(1)}$ with $f_i^{(1)}$ being the *non-equilibrium* part of the distribution, the LBGK equation also has the equivalent form:

$$f_i(\mathbf{x} + \xi_i, t + 1) = f_i^{(0)} + (1 - \omega) f_i^{(1)}. \quad (17)$$

B. Regularization and the general MRT model

Eqs. (13) and (14) also provide a natural decomposition of the discrete distribution, f_i , into components corresponding to the moments. Substituting Eq. (13) into Eq. (14), we have:

$$f_i = w_i \sum_{n=0}^N \frac{1}{n!} \sum_{j=1}^d \mathcal{H}^{(n)}(\xi_j) : \mathcal{H}^{(n)}(\xi_i) f_j. \quad (18)$$

Defining the $d \times d$ *projection matrices*:

$$M_{ij}^{(n)} = \frac{w_i}{n!} \mathcal{H}^{(n)}(\xi_i) : \mathcal{H}^{(n)}(\xi_j), \quad (19)$$

$M_{ij}^{(n)} f_j$ is the component of f_i corresponding to the n -th moment. Summing up the leading N components, we have the *regularization* operator:

$$\hat{f}_i = \sum_{n=0}^N M_{ij}^{(n)} f_j, \quad (20)$$

which takes a discrete distribution and trims its Hermite components higher than N . A regularized BGK model similar to that of Ref. [11] can then be generally written as:

$$f_i(\mathbf{x} + \boldsymbol{\xi}_i, t + 1) = (1 - \omega) \widehat{f}_i + \omega f_i^{(0)}. \quad (21)$$

The collision term on the r.h.s. is characterized by three parameters: the collision frequency, ω , the projection order, N , and the truncation order of $f^{(0)}$, M , which is not necessarily the same as N . In case f_i contains no moments beyond the N -th order, $\widehat{f}_i = f_i$. Obviously, when $M \leq N$, we have:

$$\widehat{f_i^{(0)}} = f_i^{(0)}. \quad (22)$$

In that case, Eq. (21) can be written as:

$$f_i(\mathbf{x} + \boldsymbol{\xi}_i, t + 1) = f_i^{(0)} + (1 - \omega) \widehat{f_i^{(1)}}, \quad (23)$$

which is essentially an SRT regularized LB that discards all components of the distribution that correspond to moments higher than what can be accurately represented by f_i .

By assigning a separate relaxation time to each of the Hermite components of $f^{(1)}$, the previous MRT LB model [15] can be written as:

$$f_i(\mathbf{x} + \boldsymbol{\xi}_i, t + 1) = f_i^{(0)} + \sum_{n=2}^N (1 - \omega_n) M_{ij}^{(n)} f_j^{(1)}, \quad (24)$$

where the summation starts from two because the zeroth and first moments of $f^{(1)}$ vanish due to mass and momentum conservation.

C. The multi-relaxation-time collision model

We now turn to the conditions for the collision operator to yield NSF equations by examining how the NSF equations are derived with the BGK collision model [35]. The hydrodynamic equations are the conservation laws of mass, momentum and energy, all velocity moments. Taking these moments of Eq. (2), the right-hand-side vanishes, and the left-hand-side contains the following additional central moments:

$$\boldsymbol{\sigma} = \int f c c d\mathbf{c}, \quad \text{and} \quad \mathbf{q} = \frac{1}{2} \int f c^2 c d\mathbf{c}, \quad (25)$$

which are identified as the *pressure tensor* and *heat flux*. We need to express $\boldsymbol{\sigma}$ and \mathbf{q} in terms of ρ , \mathbf{u} , θ and their derivatives to close the conservation equations. At the zeroth order, f is taken to

be the local Maxwellian of Eq. (4) which yields $\boldsymbol{\sigma}^{(0)} = \rho\theta\boldsymbol{\delta}$ and $\mathbf{q}^{(0)} = \mathbf{0}$. On substituting into the conservation equations, we have Euler's equations. Next, on substituting $f = f^{(0)} + f^{(1)}$ into Eq. (2) and ignoring $f^{(1)}$ on the left-hand-side, we have:

$$\left(\frac{\partial}{\partial t} + \boldsymbol{\xi} \cdot \nabla + \mathbf{g} \cdot \nabla_{\boldsymbol{\xi}} \right) f^{(0)} \cong -\omega f^{(1)}. \quad (26)$$

The first approximation, $f^{(1)}$, can be obtained after expressing the l.h.s. in terms of ρ , \mathbf{u} , θ and their spatial derivatives by the chain rule of differentiation and the Euler's equation. Taking the corresponding moments, we have:

$$\sigma_{ij}^{(1)} = -\tau\rho\theta \left[\frac{\partial u_i}{\partial x_j} + \frac{\partial u_j}{\partial x_i} - \frac{2}{D}\delta_{ij}\nabla \cdot \mathbf{u} \right], \quad (27a)$$

$$\mathbf{q}^{(1)} = -\frac{D+2}{2}\tau\rho\theta\nabla\theta. \quad (27b)$$

On substituting the above into the conservation equations we have the NSF equations.

Evident from this procedure is that the form of the hydrodynamic equations is completely determined by $\boldsymbol{\sigma}^{(1)}$ and $\mathbf{q}^{(1)}$. As long as the collision term satisfies the following condition:

$$\int \Omega \mathbf{c}^n d\mathbf{c} = -\omega_n \int f^{(1)} \mathbf{c}^n d\mathbf{c}, \quad \text{for } n = 2, 3. \quad (28)$$

$\boldsymbol{\sigma}^{(1)}$ and $\mathbf{q}^{(1)}$ will have the same form as Eqs. (27) with ω replaced by ω_2 and ω_3 respectively. The hydrodynamic equations will be the same NSF equations but separately tunable viscosity and thermal diffusivity. More generally, it is natural to demand that Eq. (28) is satisfied for all n . This way, each of the CM's is relaxed at its own rate. Since the set of monomials, $\{\mathbf{c}^n\}$, is a complete basis of the functional space, by specifying all moments of Ω , we specify Ω itself completely.

We now construct the collision operator in terms of its Hermite coefficients. Let the n -th Hermite coefficients of Ω and $f^{(1)}$ in absolute frame be denoted by $\mathbf{a}_{\Omega}^{(n)}$ and $\mathbf{a}_1^{(n)}$ respectively, and those in the relative frame by $\mathbf{b}_{\Omega}^{(n)}$ and $\mathbf{b}_1^{(n)}$. Due to the conservations of mass and momentum, we must have $\mathbf{a}_1^{(0)} = \mathbf{a}_1^{(1)} = 0$, and hence $\mathbf{a}_{\Omega}^{(0)} = \mathbf{a}_{\Omega}^{(1)} = 0$. By Eqs. (A6a), we have $\mathbf{b}_1^{(0)} = \mathbf{b}_1^{(1)} = \mathbf{b}_{\Omega}^{(0)} = \mathbf{b}_{\Omega}^{(1)} = 0$, and:

$$\mathbf{b}^{(2)} = \mathbf{a}^{(2)}, \quad (29a)$$

$$\mathbf{b}^{(3)} = \mathbf{a}^{(3)} - 3\mathbf{u}\mathbf{a}^{(2)}, \quad (29b)$$

$$\mathbf{b}^{(4)} = \mathbf{a}^{(4)} - 4\mathbf{u}\mathbf{a}^{(3)} + 6\mathbf{u}^2\mathbf{a}^{(2)}. \quad (29c)$$

The Hermite expansions of Ω and $f^{(1)}$ in the relative frame are:

$$\Omega = \omega(\mathbf{c}) \sum_{n=2}^N \frac{1}{n!} \mathbf{b}_{\Omega}^{(n)} : \mathcal{H}^{(n)}(\mathbf{c}), \quad (30a)$$

$$f^{(1)} = \omega(\mathbf{c}) \sum_{n=2}^N \frac{1}{n!} \mathbf{b}_1^{(n)} : \mathcal{H}^{(n)}(\mathbf{c}). \quad (30b)$$

Writing \mathbf{c}^n in terms of $\mathcal{H}^{(n)}(\mathbf{c})$ by Eqs. (A3) and using the orthogonality relations, we have:

$$\int \Omega \mathbf{c}^2 d\mathbf{c} = \frac{1}{2!} \mathbf{b}_{\Omega}^{(2)}, \quad (31a)$$

$$\int \Omega \mathbf{c}^3 d\mathbf{c} = \frac{1}{3!} \mathbf{b}_{\Omega}^{(3)}, \quad (31b)$$

$$\int \Omega \mathbf{c}^4 d\mathbf{c} = \frac{1}{4!} \mathbf{b}_{\Omega}^{(3)} + \frac{6}{2!} \delta \mathbf{b}_{\Omega}^{(2)}, \quad (31c)$$

and similar expressions for $\int f^{(1)} \mathbf{c}^n d\mathbf{c}$. On substituting into Eq. (28), we arrive at a hierarchy of equations of which the leading few are:

$$\mathbf{b}_{\Omega}^{(2)} = -\omega_2 \mathbf{b}_1^{(2)}, \quad (32a)$$

$$\mathbf{b}_{\Omega}^{(3)} = -\omega_3 \mathbf{b}_1^{(3)}, \quad (32b)$$

$$\mathbf{b}_{\Omega}^{(4)} + 72\delta \mathbf{b}_{\Omega}^{(2)} = -\omega_4 \left[\mathbf{b}_1^{(4)} + 72\delta \mathbf{b}_1^{(2)} \right]. \quad (32c)$$

Converting $\mathbf{b}^{(n)}$ to $\mathbf{a}^{(n)}$ using Eq. (29), we have:

$$\mathbf{a}_{\Omega}^{(2)} = -\omega_2 \mathbf{a}_1^{(2)}, \quad (33a)$$

$$\mathbf{a}_{\Omega}^{(3)} - 3\mathbf{u} \mathbf{a}_{\Omega}^{(2)} = -\omega_3 \left[\mathbf{a}_1^{(3)} - 3\mathbf{u} \mathbf{a}_1^{(2)} \right], \quad (33b)$$

$$\begin{aligned} \mathbf{a}_{\Omega}^{(4)} - 4\mathbf{u} \mathbf{a}_{\Omega}^{(3)} + 6(\mathbf{u}^2 + 12\delta) \mathbf{a}_{\Omega}^{(2)} = \\ -\omega_4 \left[\mathbf{a}_1^{(4)} - 4\mathbf{u} \mathbf{a}_1^{(3)} + 6(\mathbf{u}^2 + 12\delta) \mathbf{a}_1^{(2)} \right]. \end{aligned} \quad (33c)$$

Straightforwardly, $\mathbf{a}_{\Omega}^{(n)}$ can be solved as:

$$\mathbf{a}_{\Omega}^{(2)} = -\omega_2 \mathbf{a}_1^{(2)}, \quad (34a)$$

$$\mathbf{a}_{\Omega}^{(3)} = -\omega_3 \mathbf{a}_1^{(3)} + 3(\omega_3 - \omega_2) \mathbf{u} \mathbf{a}_1^{(2)}, \quad (34b)$$

$$\begin{aligned} \mathbf{a}_{\Omega}^{(4)} = -\omega_4 \mathbf{a}_1^{(4)} + 4(\omega_4 - \omega_3) \mathbf{u} \mathbf{a}_1^{(3)} \\ - 6[(\omega_4 + \omega_2 - 2\omega_3) \mathbf{u}^2 + 12(\omega_4 - \omega_2) \delta] \mathbf{a}_1^{(2)}, \end{aligned} \quad (34c)$$

which are the Hermite coefficients of Ω in the absolute frame. For comparison, the similar coefficients of the BGK and the high-order MRT [15] operators are respectively:

$$\mathbf{a}_{\Omega}^{(n)} = -\omega \mathbf{a}_1^{(n)}, \quad \text{and} \quad \mathbf{a}_{\Omega}^{(n)} = -\omega_n \mathbf{a}_1^{(n)}. \quad (35)$$

We first note that when all the relaxation times are the same, all three are identical. Second, as far as the second moments are concerned, relaxations of the central and raw moments are equivalent. This is in agreement with some of the numerical observation [29]. Third, the correction to the third moments, *i.e.*, the second term on the right-hand-side of Eq. (34b), recovers the result in Ref. [16].

The computation of the collision process goes as the following. Given the post-streaming distribution, f_i , its non-equilibrium part is $f_i^{(1)} = f_i - f_i^{(0)}$, from which $\mathbf{a}_1^{(n)}$, and $\mathbf{a}_\Omega^{(n)}$ in turn, can be calculated by Eqs. (13) and (34). Ω_i is then obtained from $\mathbf{a}_\Omega^{(n)}$ using Eq. (14), and finally the post-collision distribution is updated using the following lattice Boltzmann equation:

$$f_i(\mathbf{x} + \boldsymbol{\xi}_i, t + 1) = \hat{f}_i + \Omega_i. \quad (36)$$

III. NUMERICAL VERIFICATION

In this section we numerically verify the CM-based MRT (CM-MRT) model. First the viscosity and thermal diffusivity were numerically measured *via* the dynamics of the linear hydrodynamic modes in the presence of a translational flow. The numerical measurements are then compared with theoretical values. The independence of the transport coefficients on the translational flow, and hence the Galilean invariance in the dissipation terms, can then be verified. Secondly, a thorough and complete characterization of CM-MRT's numerical stability is beyond the scope of the present paper and deferred to a later publication. Here we choose to only present some preliminary results on the popular test case of the double shear layer [44, 45]. The results seem to show that the CM-MRT is at least as stable as the regularized collision models.

A. Linear hydrodynamic modes test

We first give the theoretical predictions of the viscous, thermal and acoustic modes in the presence of a translational flow. Consider a small perturbations on top of a base flow with constant velocity. The density, velocity and temperature, all non-dimensionalized by the scheme in Ref. [34], are written as:

$$\rho = \rho_0 + \rho', \quad \mathbf{u} = \mathbf{u}_0 + \mathbf{u}', \quad \text{and} \quad \theta = \theta_0 + \theta'. \quad (37)$$

where the subscript $_0$ and the primes denote the quantities of the base flow and the perturbation respectively. The perturbation is in the form of a monochromatic wave:

$$\begin{pmatrix} \rho' \\ \mathbf{u}' \\ \theta' \end{pmatrix} = \begin{pmatrix} \tilde{\rho} \\ \tilde{\mathbf{u}} \\ \tilde{\theta} \end{pmatrix} e^{\omega t + i\mathbf{k} \cdot (\mathbf{x} - \mathbf{u}_0 t)}, \quad (38)$$

where $\tilde{\rho}$, $\tilde{\mathbf{u}}$ and $\tilde{\theta}$ are constant scalar amplitudes of the perturbations, ω and \mathbf{k} the frequency and wave vector, and \mathbf{x} the spatial coordinate. We first decompose the velocity perturbation into components parallel and perpendicular to the wave vector, *i.e.*, we write $\tilde{\mathbf{u}} = \tilde{u}_{\parallel} \mathbf{e}_{\parallel} + \tilde{u}_{\perp} \mathbf{e}_{\perp}$, where \mathbf{e}_{\parallel} and \mathbf{e}_{\perp} are unit vectors parallel and perpendicular to \mathbf{k} . On substituting Eqs. (37) and (38) into the NSF equations, we obtain an eigen-system in the linear space of $(\tilde{\rho}, \tilde{u}_{\parallel}, \tilde{\theta}, \tilde{u}_{\perp})^T$. The four eigenvalues give the dispersion relations, while the eigen-vectors define the corresponding amplitudes.

Let γ be the *heat capacity ratio*, ν and η the first and second *kinematic viscosities*, and κ the thermal diffusivity. Further non-dimensionalizing by defining the *acoustic* Reynolds and Péclet numbers as $\text{Re} = c_s/\nu k$ and $\text{Pe} = c_s/\kappa k$, where $c_s \equiv \sqrt{\gamma\theta_0}$ is the *sound speed* at temperature θ_0 . Re and Pe are related by $\text{Pe} = \text{Re} \cdot \text{Pr}$ where $\text{Pr} \equiv \nu/\kappa$ is the Prandtl number. The dimensionless dispersion relations are:

$$-\frac{\omega_v}{c_s k} = \frac{1}{\text{Re}}, \quad (39a)$$

$$-\frac{\omega_t}{c_s k} = \frac{1}{\text{Pe}} + \frac{(\gamma - 1)\lambda}{\text{Pe}^3} + \mathcal{O}\left(\frac{1}{\text{Pe}^5}\right), \quad (39b)$$

$$\begin{aligned} -\frac{\omega_{\pm}}{c_s k} &= \frac{\gamma - \lambda}{2\text{Pe}} - \frac{(\gamma - 1)\lambda}{2\text{Pe}^3} + \mathcal{O}\left(\frac{1}{\text{Pe}^5}\right) \\ &\pm i \left[1 - \frac{(\gamma + \lambda)^2 - 4\lambda}{8\text{Pe}^2} + \mathcal{O}\left(\frac{1}{\text{Pe}^4}\right) \right], \end{aligned} \quad (39c)$$

where ω_v , ω_t , and ω_{\pm} are the angular frequencies of the viscous, thermal, and acoustic modes respectively, $\lambda \equiv 1 + (\gamma - 3)\text{Pr}$ is a constant defined for brevity. Note that while the dispersion relation of the viscous mode is exact, the other three are solutions of a cubic characteristic equation and only their asymptotic expansions at the small-Pe limit are given.

The numerical measurements were carried out as the following. First, given the desired amplitudes of the four modes, $\tilde{\rho}$, $\tilde{\mathbf{u}}$ and $\tilde{\theta}$ were determined as the superposition of the four eigen-vectors. The perturbations, ρ' , \mathbf{u}' and θ' , were then constructed according to Eqs. (38). Subsequently the amplitudes were determined by performing a spatial fast Fourier transform on a corresponding data field to extract the component of the given wave number. Noting that sound propagation is

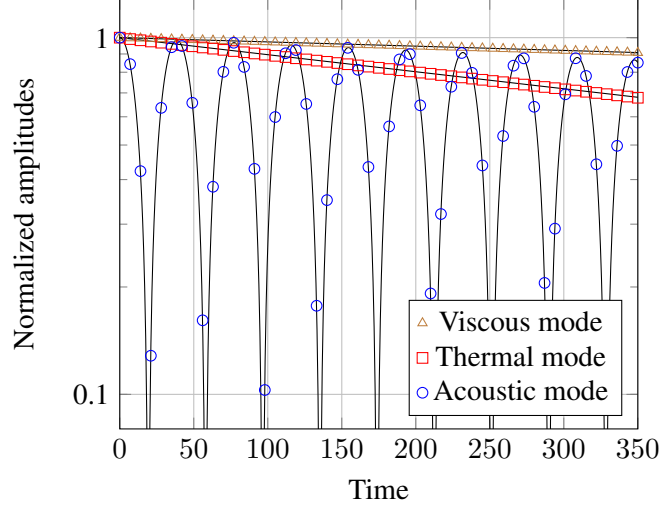


FIG. 1. Typical time histories of the linear mode amplitudes. The simulation was performed using the 2D 37-velocity $E_{2,9}^{37}$ quadrature [43] on a 100×100 double periodic lattice. Shown are the absolute values of the amplitudes of the viscous, thermal and standing acoustic waves all normalized with their initial values. The solid lines are theoretical results and symbols numerical measurements.

isentropic and thermal diffusion is isobaric, the data field for the viscous, thermal, and acoustic modes is u_{\perp} , the pressure, $p \equiv \rho\theta$, and entropy, $s \equiv c_v \ln(\theta\rho^{1-\gamma})$, respectively.

Shown in Fig. 1 is the typical behavior of the linear mode amplitudes against their theoretical values. The CM-MRT model with a ninth-order 37-speed quadrature is used. The simulation was performed with $\nu = 0.1$ and $\kappa = 0.2$, yielding a Prandtl number of 0.5. The density, temperature and translational velocity of the base flow are $\rho_0 = 1$, $\theta_0 = 1.2$ and $\mathbf{u}_0 = \mathbf{0}$ with the initial perturbation being a superposition of three monochrome viscous, thermal and standing acoustic wave, all with amplitude 0.001 and wave number $(1, 0)$, $(1, 1)$ and $(1, 0)$ respectively. The time histories were then fitted with the theoretical model of Eq. (38) to determine the angular frequencies. Comparing with Eqs. (39), the errors in ω_v , ω_t and the real and imaginary parts of ω_{\pm} are respectively 0.17%, 0.19%, 0.19% and 0.01%.

Using this measurement mechanism, we first tested the grid convergence of the CM-MRT model with a number of high-order quadratures. As previously shown [43], high-order quadrature rules with abscissas coincide with lattice nodes (on-lattice) that can accurately represent moments of any order can be found by solving a linear programming problem. The solutions form a polytope in the parameter space with its vertexes representing the quadratures with minimum number of velocities. In 2D, the minimum 7-th degree quadrature rules are the four $E_{2,17}^7$ rules, and the

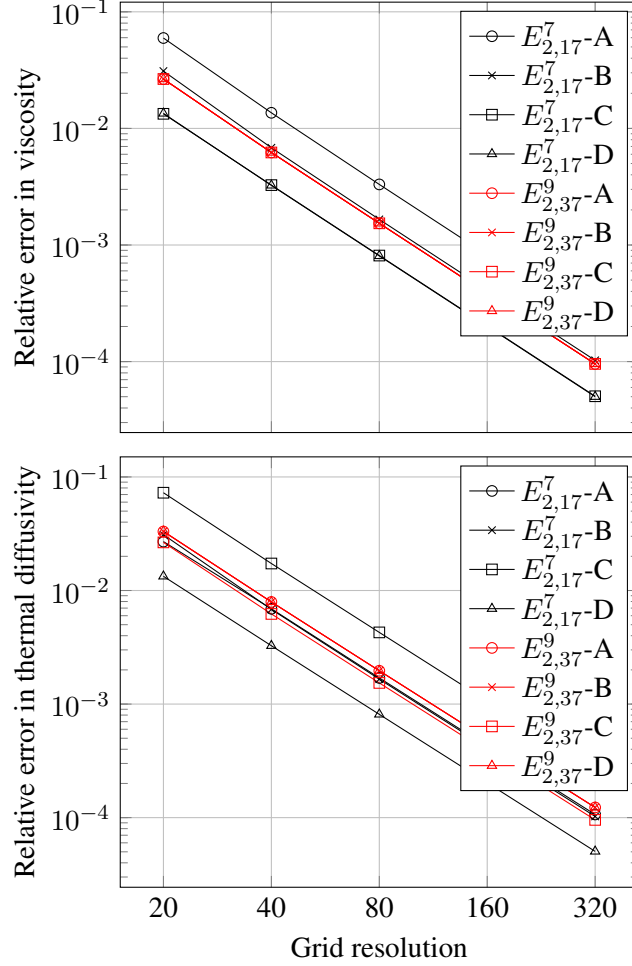


FIG. 2. Grid convergence of the CM-MRT model. Plotted are the relative errors in viscosity (top) and thermal diffusivity (bottom) using the $E_{2,17}^7$ and $E_{2,37}^9$ quadratures on a $L \times L$ lattice ranging from $L = 20$ to $L = 320$. The errors in viscosity of the four $E_{2,37}^9$ quadrature are almost identical and coincide on the graph. Although all models are second order, the magnitudes of the error can differ by a factor of approximately 4-5 among all quadrature rules. The quadrature $E_{2,17}^7$ -D is found to have the best accuracy.

minimum 9-th degree rules are the four $E_{3,37}^9$ rules, all given in Ref. [43]. Shown in Fig. 2 are the relative errors in viscosity and thermal diffusivity measured by linear mode simulations using the CM-MRT model with all eight quadratures. All models demonstrate a second order spatial accuracy with the one using quadrature $E_{2,17}^7$ -D being the most accurate.

We then used this apparatus to verify the Galilean invariance by including a translational velocity in the base flow, in a similar fashion as in Ref. [16]. Specifically we set $\mathbf{u}_0 = (0, u_0)$, and the initial perturbation consists of a viscous and a thermal wave, both with wave vector $\mathbf{k} = (1, 0)$

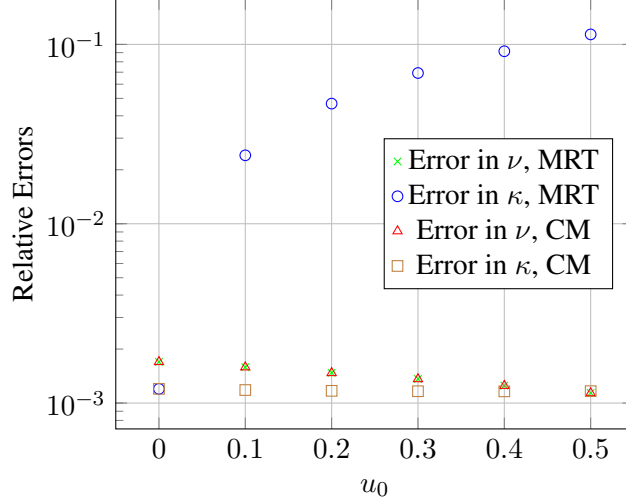


FIG. 3. Restoration of the Galilean invariance of transport coefficients by the CM-MRT model. Plotted are the relative errors in viscosity, ν , and thermal diffusivity, κ , as measured from the linear mode tests using MRT and CM-MRT models, both with the $E_{2,9}^{37}$ quadrature on a 100×100 lattice. On the horizontal axis is the magnitude of the translational velocity. The error in thermal diffusivity in the MRT model increases with u_0 , breaking the Galilean invariance.

and initial amplitude of 0.001. The base flow is in the transverse direction of the wave vector. Shown in Fig. 3 are the errors in the measured viscosity and thermal diffusivity against u_0 using the MRT [15] and CM-MRT models. To be seen is that the errors in viscosity are small and identical, confirming the theoretical finding that the relaxations of raw and central moments at the second order are identical. The error in thermal diffusivity in MRT however increases linearly with u_0 . This violation of Galilean invariance is eliminated in CM-MRT.

B. Double shear layer test

The double-shear-layer (DSL) [44, 45] is a well studied test case for numerical stability benchmark [13, 14, 46–49]. The two-dimensional flow field is defined on a double periodic domain $0 \leq x, y \leq 1$ by:

$$u_x = \begin{cases} u_0 \tanh \rho(y - \frac{1}{4}), & y \leq \frac{1}{2} \\ u_0 \tanh \rho(\frac{3}{4} - y), & y > \frac{1}{2} \end{cases}, \quad (40a)$$

$$u_y = \delta u_0 \sin 2\pi \left[x + \frac{1}{4} \right], \quad (40b)$$

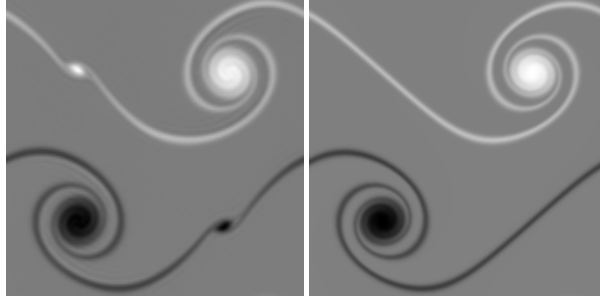


FIG. 4. Vorticity field at $t = 1$ in a double shear layer simulation using the D2Q9 BGK model. On the left, the simulation resolution is 128×128 , deemed insufficient as indicated by the spurious secondary vortices that are absent in the better resolved case (256×256) on the right. The Reynolds number and Mach number are respectively 10,000 and 0.1 in both cases.

where $1/\rho$ measures the thickness of the shear layer, and δ a small parameter controlling the magnitude of the initial vertical perturbation. In simulations here, we chose $\rho = 80$ and $\delta = 0.05$ in accordance with the literature. All simulations are performed on a $L \times L$ square lattice where L is the number of sites in one direction. In our notation [34], lengths are scaled by the lattice constant, c , and velocities by the isothermal sound speed, c_s . The Reynolds and Mach numbers are therefore $\text{Re} = u_0 c L / \nu$ and $\text{Ma} = u_0$. Shown in Fig. 4 are the typical vorticity fields simulated using D2Q9 with the resolutions $L = 128$ and $L = 256$ respectively. The occurrence of the secondary vortices on the left is a well-known indication of insufficient resolution.

Extensive studies on the DSL were carried out to benchmark various collision models [13, 14]. For comparison, we also computed the stability boundary of the DSL using the isothermal MRT, isothermal CM-MRT and full thermal CM-MRT models on the same $L = 128$ lattice. For a fixed pair of Pr and Re , the maximum Ma is defined as the highest Ma that allows the simulation to be stably carried out till $t/t_c = 2$ [14]. An iterative search algorithm was used to found the maximum Ma for fixed Pr and Re . Shown in Fig. 5 are the time histories of the averaged kinetic energy, $\langle u^2 \rangle / u_0^2$, for an increasing sequence of Mach numbers at $\text{Pr} = 1$ and $\text{Re} = 10^7$ using the thermal CM-MRT. The maximum Ma is determined at 0.2688 in this case.

Shown in Fig. 6 are the stability boundaries in the Re - Ma plane using, from top to bottom, isothermal MRT, isothermal CM-MRT, and full thermal CM-MRT models. The same $E_{2,37}^9$ -A quadrature was used in all cases and the truncation levels were $M = N = 4$. In the isothermal cases, the temperature field was frozen at unity so that heat transfer is not simulated and τ_3 becomes

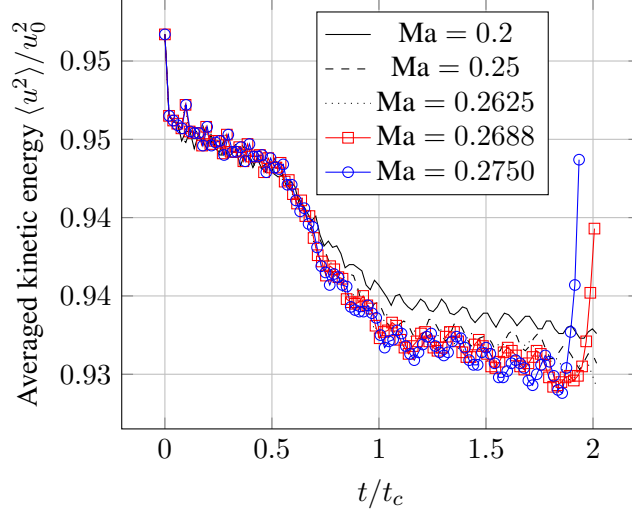


FIG. 5. (Color online) Time histories of the averaged kinetic energy normalized by its initial value for a sequence of Mach number at $\text{Pr} = 1$ and $\text{Re} = 10^7$ using thermal CM-MRT on an 128×128 lattice. At $\text{Ma} = 0.275$ the simulation diverged and at 0.2688 it barely survived beyond $t/t_c = 2$.

a free parameter with no direct impact on the hydrodynamic equations. To study its effect on numerical stability, the stability boundaries are plotted for a range of Prandtl numbers defined as $\text{Pr} \equiv \nu/\kappa$. It is evident from Fig. 6 that for the isothermal simulations with τ_3 not too far from τ_2 , the MRT and CM-MRT perform similarly in terms of achievable Mach number and Reynolds number. Comparing with the best result of the regularized LBGK models [13, 14], the present result ($\text{Ma} \sim 0.7$) is approximately 20% better. For comparison, in the full thermal case, the maximum achievable Ma number drops to ~ 0.25 over a wide range of Prandtl number. Nevertheless, taking into account that the grid is severely under-resolved, this maximum is by no means implied as a limit in practical simulations.

IV. CONCLUSIONS AND DISCUSSION

In summary, we propose a multiple-relaxation-time collision model by relaxing the central moments of the distribution function with individually assigned rates. The collision model is constructed in a way that guarantees that Chapman-Enskog calculation yields the correct hydrodynamic equation with separately tunable transport coefficients. Using binomial transform, the central moments are converted to raw moments for use in lattice Boltzmann models. It is theoretically shown and numerically verified that viscous and thermal dissipations are Galilean invariant

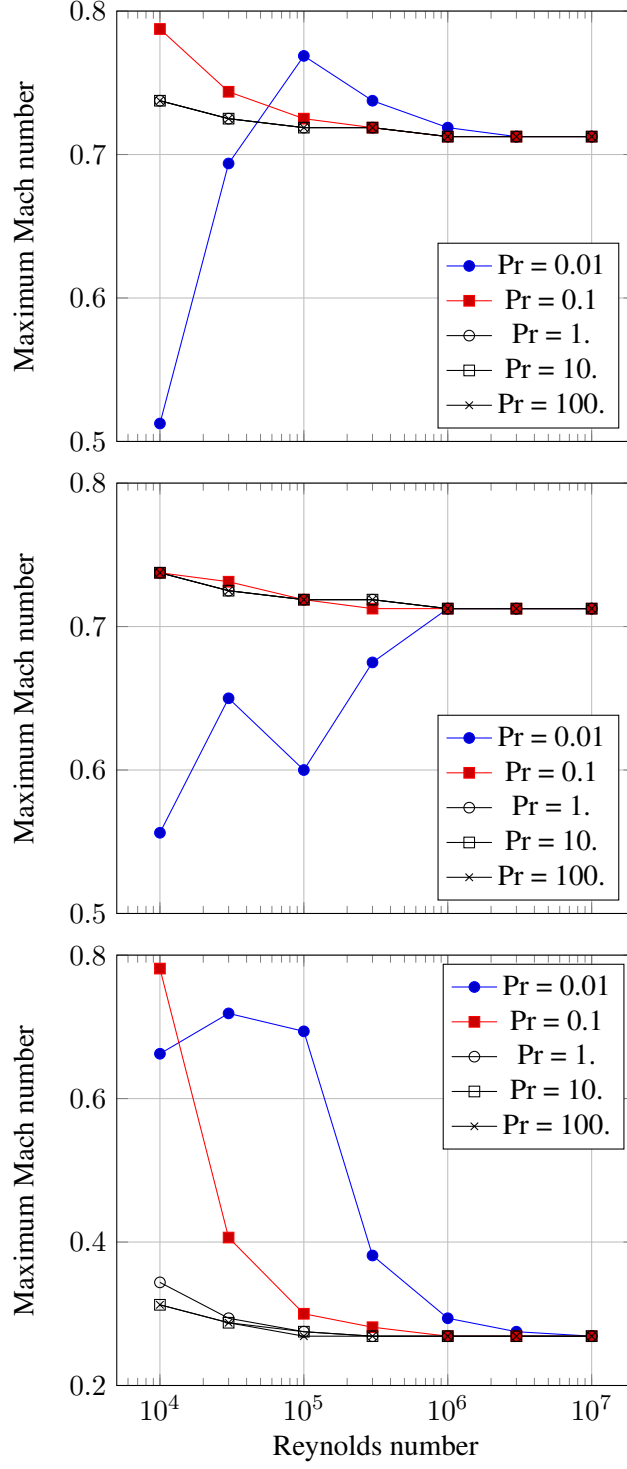


FIG. 6. Stability boundaries in the double shear layer simulation using isothermal MRT (top), isothermal CM-MRT (middle) and thermal CM-MRT (bottom) models. On the y -axis is the maximum Mach number (u_0) that the simulation can be carried out to $u_0 t / Lc = 2$. For comparison, the Prandtl number is used as a measure of τ_3 relative to τ_2 in the top two isothermal cases although heat transfer is not simulated there.

and mutually independent, allowing a variable Prandtl number in CFD simulations. The derivation is simple, lattice-independent and applicable to moments of any order. Excellent numerical stability was also observed in the double-shear-layer test case.

ACKNOWLEDGMENTS

This work was supported by the National Science Foundation of China Grants 91741101.

Appendix A: Hermite expansions in the absolute and relative frames

The tensorial Hermite polynomials can be defined by the *recursive relation*:

$$\boldsymbol{\xi} \mathcal{H}^{(n)}(\boldsymbol{\xi}) = \mathcal{H}^{(n+1)}(\boldsymbol{\xi}) + n\boldsymbol{\delta} \mathcal{H}^{(n-1)}(\boldsymbol{\xi}), \quad (\text{A1})$$

where $\boldsymbol{\delta}$ is the rank-2 identity tensor. The first few are:

$$\mathcal{H}^{(0)}(\boldsymbol{\xi}) = 1, \quad (\text{A2a})$$

$$\mathcal{H}^{(1)}(\boldsymbol{\xi}) = \boldsymbol{\xi}, \quad (\text{A2b})$$

$$\mathcal{H}^{(2)}(\boldsymbol{\xi}) = \boldsymbol{\xi}^2 - \boldsymbol{\delta}, \quad (\text{A2c})$$

$$\mathcal{H}^{(3)}(\boldsymbol{\xi}) = \boldsymbol{\xi}^3 - 3\boldsymbol{\xi}\boldsymbol{\delta}, \quad (\text{A2d})$$

$$\mathcal{H}^{(4)}(\boldsymbol{\xi}) = \boldsymbol{\xi}^4 - 6\boldsymbol{\xi}^2\boldsymbol{\delta} + 3\boldsymbol{\delta}^2. \quad (\text{A2e})$$

Inversely, the monomials can be expressed by the Hermite polynomials:

$$1 = \mathcal{H}^{(0)}(\boldsymbol{\xi}), \quad (\text{A3a})$$

$$\boldsymbol{\xi} = \mathcal{H}^{(1)}(\boldsymbol{\xi}), \quad (\text{A3b})$$

$$\boldsymbol{\xi}^2 = \mathcal{H}^{(2)}(\boldsymbol{\xi}) + \boldsymbol{\delta} \mathcal{H}^{(0)}(\boldsymbol{\xi}), \quad (\text{A3c})$$

$$\boldsymbol{\xi}^3 = \mathcal{H}^{(3)}(\boldsymbol{\xi}) + 3\boldsymbol{\delta} \mathcal{H}^{(1)}(\boldsymbol{\xi}), \quad (\text{A3d})$$

$$\boldsymbol{\xi}^4 = \mathcal{H}^{(4)}(\boldsymbol{\xi}) + 6\boldsymbol{\delta} \mathcal{H}^{(2)}(\boldsymbol{\xi}) + 3\boldsymbol{\delta}^2 \mathcal{H}^{(0)}(\boldsymbol{\xi}). \quad (\text{A3e})$$

In statistics, the *central* and *raw* moments of a distribution, defined as the moments about the mean and origin respectively, are related to each other by the *binomial transform*. Similar relations exist between the Hermite polynomials and the expansion coefficients in the relative and absolute reference frames. First, the following relation can be established by induction:

$$\mathcal{H}^{(n)}(\boldsymbol{\xi} + \boldsymbol{u}) = \sum_{i=0}^n C_n^i \mathcal{H}^{(i)}(\boldsymbol{\xi}) \boldsymbol{u}^{n-i}, \quad (\text{A4})$$

where C_n^i is the *binomial coefficient*. The Hermite polynomials in the relative and absolute frames are hence related to each other by the following binomial transforms:

$$\mathcal{H}^{(n)}(\mathbf{c}) = \sum_{i=0}^n (-1)^{n-i} C_n^i \mathcal{H}^{(i)}(\boldsymbol{\xi}) \mathbf{u}^{n-i}, \quad (\text{A5a})$$

$$\mathcal{H}^{(n)}(\boldsymbol{\xi}) = \sum_{i=0}^n C_n^i \mathcal{H}^{(i)}(\mathbf{c}) \mathbf{u}^{n-i}, \quad (\text{A5b})$$

where $\mathbf{c} \equiv \boldsymbol{\xi} - \mathbf{u}$. Let $\mathbf{a}^{(n)}$ and $\mathbf{b}^{(n)}$ be respectively the Hermite coefficients in the absolute and relative frames. By Eq. (9), they are related to each other by the binomial transforms:

$$\mathbf{b}^{(n)} = \sum_{i=0}^n (-1)^{n-i} C_n^i \mathbf{a}^{(i)} \mathbf{u}^{n-i}, \quad (\text{A6a})$$

$$\mathbf{a}^{(n)} = \sum_{i=0}^n C_n^i \mathbf{b}^{(i)} \mathbf{u}^{n-i}. \quad (\text{A6b})$$

Explicitly, the leading few expressions are:

$$\mathbf{b}^{(0)} = \mathbf{a}^{(0)}, \quad (\text{A7a})$$

$$\mathbf{b}^{(1)} = \mathbf{a}^{(1)} - \mathbf{u} \mathbf{a}^{(0)}, \quad (\text{A7b})$$

$$\mathbf{b}^{(2)} = \mathbf{a}^{(2)} - 2\mathbf{u} \mathbf{a}^{(1)} + \mathbf{u}^2 \mathbf{a}^{(0)}, \quad (\text{A7c})$$

$$\mathbf{b}^{(3)} = \mathbf{a}^{(3)} - 3\mathbf{u} \mathbf{a}^{(2)} + 3\mathbf{u}^2 \mathbf{a}^{(1)} - \mathbf{u}^3 \mathbf{a}^{(0)}, \quad (\text{A7d})$$

\dots ,

and

$$\mathbf{a}^{(0)} = \mathbf{b}^{(0)}, \quad (\text{A8a})$$

$$\mathbf{a}^{(1)} = \mathbf{b}^{(1)} + \mathbf{u} \mathbf{b}^{(0)}, \quad (\text{A8b})$$

$$\mathbf{a}^{(2)} = \mathbf{b}^{(2)} + 2\mathbf{u} \mathbf{b}^{(1)} + \mathbf{u}^2 \mathbf{b}^{(0)}, \quad (\text{A8c})$$

$$\mathbf{a}^{(3)} = \mathbf{b}^{(3)} + 3\mathbf{u} \mathbf{b}^{(2)} + 3\mathbf{u}^2 \mathbf{b}^{(1)} + \mathbf{u}^3 \mathbf{b}^{(0)}, \quad (\text{A8d})$$

\dots .

-
- [1] U. Frisch, B. Hasslacher, and Y. Pomeau, Phys. Rev. Lett. **56**, 1505 (1986).
 - [2] R. Benzi, S. Succi, and M. Vergassola, Phys. Rep. **222**, 145 (1992).
 - [3] S. Chen and G. D. Doolen, Annu. Rev. Fluid Mech. **30**, 329 (1998).

- [4] P. Bhatnagar, E. P. Gross, and M. Krook, Phys. Rev. **94**, 511 (1954).
- [5] H. Chen, S. Chen, and W. H. Matthaeus, Phys. Rev. A **45**, R5339 (1992).
- [6] Y.-H. Qian, D. d’Humières, and P. Lallemand, Europhys. Lett. **17**, 479 (1992).
- [7] D. d’Humières, in *Rarefied gas dynamics: theory and simulations*, Prog. Aeronaut. Astronaut., Vol. 159, edited by B. D. Shizgal and D. P. Weaver (1992) pp. 450–458.
- [8] D. d’Humières, I. Ginzburg, M. Krafczyk, P. Lallemand, and L.-S. Luo, Philos. Trans. R. Soc. A Math. Phys. Eng. Sci. **360**, 437 (2002).
- [9] M. Geier, A. Greiner, and J. G. Korvink, Phys. Rev. E **73**, 066705 (2006).
- [10] A. J. C. Ladd, J. Fluid Mech. **271**, 285 (1994).
- [11] J. Latt and B. Chopard, Math. Comput. Simul. **72**, 165 (2006), arXiv:0506157 [physics].
- [12] H. Chen, R. Zhang, I. Staroselsky, and M. Jhon, Phys. A Stat. Mech. its Appl. **362**, 125 (2006).
- [13] K. K. Mattila, P. C. Philippi, and L. A. Hegele, Phys. Fluids **29**, 046103 (2017).
- [14] C. Coreixas, G. Wissocq, G. Puigt, J.-F. Boussuge, and P. Sagaut, Phys. Rev. E **96**, 033306 (2017).
- [15] X. Shan and H. Chen, Int. J. Mod. Phys. C **18**, 635 (2007).
- [16] H. Chen, P. Gopalakrishnan, and R. Zhang, Int. J. Mod. Phys. C **25**, 1450046 (2014).
- [17] E. P. Gross and E. A. Jackson, Phys. Fluids **2**, 432 (1959).
- [18] L. H. Holway, Phys. Fluids **9**, 1658 (1966).
- [19] P. Andries, AIP Conf. Proc. **585**, 30 (2001).
- [20] E. M. Shakhov, Fluid Dyn. **3**, 95 (1972).
- [21] G. R. McNamara, A. L. Garcia, and B. J. Alder, J. Stat. Phys. **87**, 1111 (1997).
- [22] P. Lallemand and L.-S. Luo, Phys. Rev. E **68**, 036706 (2003).
- [23] X. Nie, X. Shan, and H. Chen, Europhys. Lett. **81**, 34005 (2008).
- [24] P. Lallemand and L.-S. Luo, Phys. Rev. E **61**, 6546 (2000).
- [25] G. R. McNamara, A. L. Garcia, and B. J. Alder, J. Stat. Phys. **81**, 395 (1995).
- [26] O. P. Malaspinas, , 1 (2015), arXiv:1505.06900.
- [27] Y.-H. Qian and S. A. Orszag, Europhys. Lett. **21**, 255 (1993).
- [28] P. J. Dellar, J. Comput. Phys. **259**, 270 (2014).
- [29] Y. Ning, K. N. Premnath, and D. V. Patil, Int. J. Numer. Methods Fluids **82**, 59 (2016).
- [30] H. Grad, Commun. Pure Appl. Math. **2**, 331 (1949).
- [31] C. Sun, J. Comput. Phys. **84**, 70 (2000).
- [32] C. Sun and A. T. Hsu, Phys. Rev. E **68**, 016303 (2003).

- [33] X. Shan and X. He, Phys. Rev. Lett. **80**, 65 (1998).
- [34] X. Shan, X.-F. Yuan, and H. Chen, J. Fluid Mech. **550**, 413 (2006).
- [35] K. Huang, *Statistical Mechanics*, 2nd ed. (John Wiley & Sons, New York, 1987).
- [36] S. Chapman and T. G. Cowling, *The Mathematical Theory of Non-Uniform Gases*, 3rd ed. (Cambridge University Press, London, 1970).
- [37] H. Grad, Commun. Pure Appl. Math. **2**, 325 (1949).
- [38] V. I. Krylov, *Approximate Calculation of Integrals* (MacMillan, 1962).
- [39] A. H. Stroud, *Approximate Calculation of Multiple Integrals* (Prentice-Hall, Englewood Cliffs, N.J., 1971).
- [40] P. C. Philippi, L. Hegele, L. O. E. dos Santos, and R. Surmas, Phys. Rev. E **73**, 056702 (2006).
- [41] S. S. Chikatamarla and I. V. Karlin, Phys. Rev. E **79**, 46701 (2009).
- [42] X. Shan, Phys. Rev. E **81**, 036702 (2010).
- [43] X. Shan, J. Comput. Sci. **17**, 475 (2016).
- [44] D. L. Brown and M. L. Minion, J. Comput. Phys. **122**, 165 (1995).
- [45] M. L. Minion and D. L. Brown, J. Comput. Phys. **138**, 734 (1997).
- [46] P. J. Dellar, Phys. Rev. E **64**, 031203 (2001).
- [47] P. J. Dellar, J. Comput. Phys. **190**, 351 (2003).
- [48] F. Bösch, S. S. Chikatamarla, and I. V. Karlin, ESAIM Proc. Surv. **52**, 1 (2015), arXiv:1507.02509.
- [49] K. K. Mattila, L. A. Hegele, and P. C. Philippi, Phys. Rev. E **91**, 063010 (2015).